Topology Modeling and Design of a Novel Magnetic Coupling Fault Current Limiter for VSC DC Grids

Zipan Nie, Zhanqing Yu, *Member, IEEE*, Zhizheng Gan, Lu Qu, Yulong Huang, *Member, IEEE*, and Biao Zhao, *Senior Member, IEEE*

***Abstract*—In a voltage-source converter dc grid, a dc fault current limiter (FCL) is a key apparatus. When faults occur, it is supposed to effectively and immediately suppress transient short-circuit current to protect other equipment, e.g., converters. Additionally, it is required to bring as little negative effect as possible under normal operation. Although the respective advantages are highlighted in different FCLs, one or two key disadvantages can significantly decrease the overall performance. In this article, a novel magnetic coupling FCL (MCFCL) is proposed and achieves a good balance among its advantages and disadvantages. An MCFCL consists of a mutual inductor and some power electronic switch modules. The mutual inductor metallic primary winding is connected in series to the transmission line and magnetically coupled with the secondary winding. The secondary side impedance is controlled by the power electronic switch modules. The novel 4-segment model is proposed to demonstrate the current-limiting physics, formulate the current-limiting effect, and support the design. One medium voltage (10 kV) case study is carried out based on the numerical simulation. The MCFCL shows a better current-suppressing effect and a lower impedance under normal operation than the benchmark Reactor FCL. Finally, this article is validated on a scaled-down experimental facility.**

***Index Terms*—DC power transmission, electromagnetic coupling, fault current limiters, short-circuit currents.**

I. Introduction

EITHER an ac FCL or dc FCL is supposed to limit short-circuit current before ac or dc circuit breaker (ACCB or DCCB) interruption. However, their current-limiting requirements and operation conditions are different. A conventional ac grid is more robust to short-circuit current than a voltage-source converter (VSC) dc grid, and moreover high inductive components in ac grids can limit transient overcurrent. An ACCB is rated to the worst-case steady-state fault current while a DCCB has the rating much lower than the worst-case steady-state dc fault current due to technical limitations and economic considerations. Hence, DCCBs must response fast before any destructive consequence occurs [1]. Usually, the ACCB interruption delay is several tens of milliseconds, and the interruption delay is about several milliseconds for DCCBs [1]. In the latest DCCB technology, a current-limiting inductor of 50–300 mH is required to be connected in series to a VSC HVdc DCCB to limit the peak current. While the introduction of inductance worsens dc grid voltage control precision [1]. Additionally, it decreases system dynamic characteristics. Fig. 1 shows locations of DCCBs and FCLs in a VSC dc grid and the faults (pole-to-pole or pole-to-ground short circuit) are supposed to occur on power lines between different VSC stations.

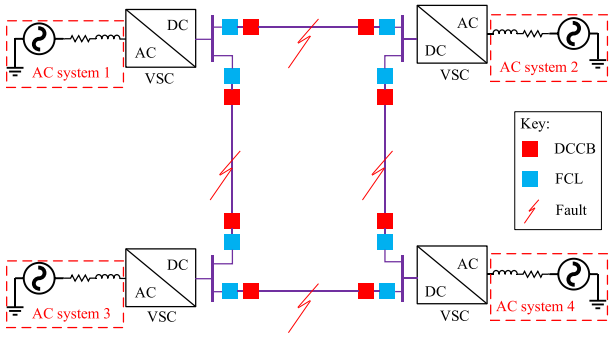

Fig. 1 Locations of FCLs in a dc grid.

An ideal dc FCL is supposed to have the following characteristics via the summary from [2]–[4].

1) Under the normal operation, an FCL is supposed to have low loss and low impedance.
2) Once a short-circuit fault initiates, an FCL is supposed to change to high impedance quickly and change back to low impedance immediately after the fault clearance. These require controllable impedance, fast response, and recovery.
3) An FCL should be able to limit fault current even under the failure of its primary mechanism, being inherent fail-safe.
4) An FCL is supposed to be compact and light.
5) An FCL is supposed to be low cost, simple, and reliable.

FCLs can be classified into superconducting FCLs and non-superconducting FCLs. Table I compares different FCLs.

Superconducting fault current limiters (SFCLs) can be categorized into saturated iron core SFCLs (SI-SFCLs), resistive SFCLs (R-SFCLs), and inductive shielded core SFCLs

Manuscript received May 6, 2020; revised August 7, 2020; accepted September 16, 2020. Date of publication September 21, 2020; date of current version November 20, 2020. This work is supported in part by the National Natural Science Foundation of China (51922062) and in part by the National Key Research Program of China under Grant 2018YFB0904600. This paper was presented in part at the 4th IEEE Workshop on the Electronic Grid Xiamen. China, in November, 2019. Recommended for publication by Associate Editor M. Tavakoli Bina. *(Corresponding authors: Zhanqing Yu; Zipan Nie.)*

The authors are with the Department of Electrical Engineering, Tsinghua University, Beijing 100084, China (e-mail: zipannie@hotmail.com; yzq@tsinghua.edu.cn; gzz16@mails.tsinghua.edu.cn; qulu@tsinghua.edu.cn; yulonghuang@mail.tsinghua.edu.cn; zhao-biao@tsinghua.edu.cn).

Color versions of one or more of the figures in this article are available online at https://ieeexplore.ieee.org.

Digital Object Identifier 10.1109/TPEL.2020.3025461

TABLE I
DIFFERENT FCLs COMPARISONS

	Superconducting			Non-superconducting				
	SI-SFCL	R-SFCL	I-SFCL	Reactor FCL	SSFCL	SI-FCL	LM-FCL	MCFCL
Loss	Low	Extremely low	Low	Low	High	High	Low	Low
Impedance under normal operation	Low	Low	Low	High	Low	Low	Low	Low
Controllable impedance	Yes	Yes	Yes	No	Yes	Yes	Yes	Yes
Response time	Immediate	Immediate	Immediate	N/A	From μs to ms	Immediate	Several microseconds	Immediate
Recovery time	Immediate	Hundreds of milliseconds	Similar with R-SFCL	N/A	Immediate	Immediate	Tens of microseconds *	Immediate
Inherent fail-safe	Yes	Yes	Yes	N/A	No	Yes	No	Yes
Size	Very big	Big	Very big	Small	Medium	Big	Small	Medium
Weight	Very heavy	Heavy	Heavy	Light	Medium	Heavy	Light	Medium
Cost	Very high	High	Very high	Low	Medium	High	Low	Medium
Complexity	Very high	High	Very High	Low	Medium	High	Low	Medium
Reliability	Low	Low	Low	High	Medium	Medium	Low	Medium

*Inquiry from the author of paper [21].

(I-SFCLs), as shown in Table I. Due to the superconducting material, extremely low loss is consumed on R-SFCLs under normal operation [2]. As both of SI-SFCLs and I-SFCLs have nonsuperconducting metallic primary windings connected to power line, they have low loss. The cryocooler power is not added into the loss, and for the other FCLs the cooling system power is not counted as well. All SFCLs have low impedance under normal operation. They can change to high impedance immediately once a fault occurs, and the response time meets the requirements for VSC dc grids. After faults, SI-SFCLs can recover immediately, while it takes time for R-SFCLs and I-SFCLs to recover [5]. The recovery time recently recorded for an R-SFCL is within 200 ms under a 10 ms current pulse with the maximum amplitude 8842 A [6]. Although the recovery time of an I-SFCL is unavailable from literatures, it should be in the same level with that of R-SFCLs. Because in both, recovery time is the time that it takes for superconducting material to recover from quenching state. In terms of the fail-safe characteristic, in [4], it is defined as "Fail safe limiting operation. This indicates whether the FCL will still limit the fault current even if its primary mechanism fails." SFCLs are fail-safe according to [2]. According to [4], [7]–[9], the sizes and weights of SFCLs and the others are given in Table I. Because superconducting material and cryocooler are both very expensive [2], [10], high cost is one problem. Moreover, the high complexity and low reliability are also the problems for SFCLs. While a 20-kV dc R-SFCL is designed and tested, and it would be installed in the live grid [11].

The simplest nonsuperconducting FCLs in VSC dc grids are current-limiting inductors, which are already deployed in existing projects [1], [12]–[14], and in this article, the current-limiting inductor is named Reactor FCL. As shown in Table I, it has low loss, small footprint [8], light weight [8], low cost, simple structure, and high reliability while its impedance is high under normal operation and not changeable. For Reactor FCLs, the higher current-limiting effect is required, the higher inductance is designed, which will result in lower dc-link voltage control precision and dc grid dynamic characteristics. This cannot be neglected in a dc grid with renewable generations of unpredictable power fluctuation and loads of frequent variation [10].

For solid-state FCLs (SSFCLs) in dc grid, it is necessary to clarify its definition. An SSFCL is an FCL that its solid-state device(s) conduct(s) all or part of the power line current under normal operation; once fault occurs the solid-state device(s) is/are switched OFF to commutate the short-circuit current to the high impedance branch. Under normal operation the loss is high due to solid-state device conduction, while the impedance is low. They can response and recover quickly as shown in Table I [7], [15]. It is not fail-safe to the solid-state device failure because under this condition the short-circuit current cannot be commutated to the high impedance branch. The cost is medium according to the material prices in [10]. The implementation of power electronic devices increases the complexity and decreases the reliability, but not much. Some new dc SSFCLs are emerging, for example, the high-inductance solid-state dc-reactor-based FCL in [16] and the mutual-inductance-type FCL in [17]. Both use the structure of power electronic devices and mutual inductors. It is claimed that their current-limiting performances are improved, compared with Reactor FCLs, while high loss is still inevitable.

Saturated iron core-type fault current limiters (SI-FCLs) have the same principle with SI-SFCLs, but superconducting material and cryocooler are not used in the dc biased winding. This brings some benefits as shown in Table I. An SI-FCL has been in live operation [18]. In [19], a novel three-limb topology saturated iron core-type fault current limiter is proposed and contains both dc coils and two kinds of permanent magnets to supply magnetomotive force. However, this needs further considerations on complexity, permanent magnet stability [20], and demagnetization.

Liquid metal FCLs (LM-FCLs) can be categorized into arc LM-FCLs [21] and arc-less LM-FCLs [4], out of which the former uses pinch-off effect to generate arc, and the later uses

magnetic force to change resistance. The arc-less LM-FCL by ABB can respond around 5–8 ms after the fault inception [22], while the arc LM-FCL in [21] has the response time of about 2 ms. It is not fail-safe to the liquid metal leakage. Its size weight and cost are good compared with the other FCLs in Table I. However, the liquid conductor and electrode corrosion decrease its reliability.

Some FCLs of other types are not included in Table I. A hybrid FCL in [23] is proposed for dc. It efficiently limits the dc fault current and decreases the DCCB interruption time and energy dissipation. However, the introduction of both mechanical switch and semiconductor devices into the power line may need some more considerations in terms of response time, loss, and reliability. A novel current-commutation-based FCL is proposed in [24] for VSC dc grid, it can avoid the negative influence from Reactor FCL and increase the fault current clearance speed. While during power flow shifting condition, high current goes through semiconductor devices, which may generate high loss and hence large amount of heat. ABB has commercialized the ac Is-limiters with the voltage rating 40.5-kV and 210-kA rms breaking capability [25], while it contains disposable components and needs manual recovery. The ac FCLs proposed in [3], [26]–[29] are composed of transformers and power electronic devices. They share the common current-limiting approach that the impedance is quickly changed via the power electronic switches and this is magnetically coupled to the other side on the transformer. The current-limiting requirements principles and performances in ac grids are different with those in VSC dc grids.

Consequently, different FCLs have their respective advantages, however even one key disadvantage can significantly decrease the overall performance. A new FCL technology should be proposed to properly balance the advantages and disadvantages. It is supposed to have a good overall good performance. Superconducting material is excluded for reliability and cost considerations. However, these demerits of superconducting material may be solved in the future.

The philosophy is considered as below to alleviate the existing FCL disadvantages, based on which the new dc current-limiting principle is proposed for VSC dc grids.

1) Any nonmetallic component should not be introduced into transmission lines by FCLs, achieving low resistance under normal operation.
2) Power electronic devices are used to achieve quick impedance change, and hence the FCL high transient response.
3) Magnetic coupling is used to couple the power electronic controlled impedance to transmission lines and electrically isolate the possible failure of the power electronic devices.

In this article, a novel magnetic coupling FCL (MCFCL) is proposed. Its primary metallic winding is connected in series to a transmission line, and the secondary side impedance is controlled by power electronic switch modules. The secondary impedance is magnetically coupled to the primary side via a mutual inductor. Herein, the mutual inductor is air-cored to realize the simplest magnetic coupling and avoid introducing

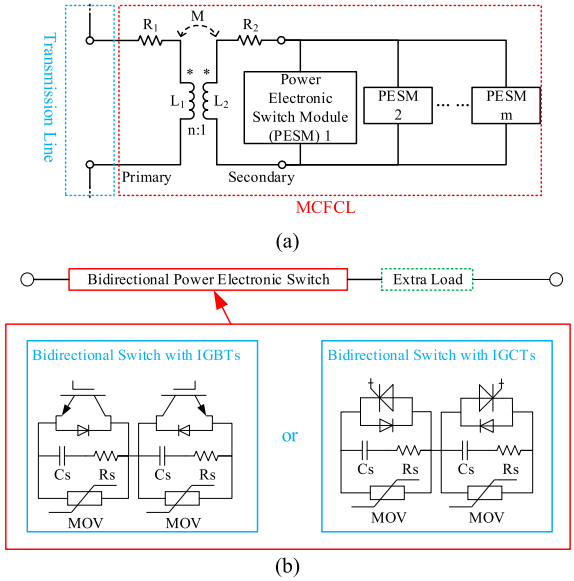

Fig. 2. MCFCL topology. (a) MCFCL topology. (b) Power electronic switch module (PESM) examples.

any other side effects, for example, iron loss and magnetic saturation. Other core types can be considered in the later research works. Under normal operation, the ohmic conduction loss on the primary winding is negligible, and once a short-circuit fault occurs the MCFCL impedance can be quickly switched to high via the power electronic switch modules. The power electronic switch modules only withstand high voltage and current during the current-limiting transient.

The rest of this article is organized as follows. In Section I, different FCL technologies are reviewed, the novel MCFCL is introduced, and the article is outlined, which is followed by MCFCL topology performance and modeling in Section II. The MCFCL design case study is discussed in Section III, which is followed by the experimental validation in Section IV. Finally, the conclusion is given in Section V.

II. MCFCL Topology Performance and Modeling

The MCFCL topology is demonstrated first, the foundation, and core idea of this article, which is followed by the MCFCL analytical modeling, the mathematical tool to analyze its performance and design it. The MCFCL analytical model is newly proposed and named four-segment model.

A. MCFCL Topology

The topology of MCFCL is shown in Fig. 2(a). It contains a mutual inductor whose primary winding is connected to the transmission line and the secondary to power electronic switch modules. The secondary impedance can be quickly changed by power electronic switch modules with fully controlled power electronic devices, e.g., integrated gate commutate thyristors (IGCTs) or insulated gate bipolar transistors (IGBTs). Through the magnetic coupling between the primary and secondary winding, the MCFCL impedance can be changed quickly. Two

examples of power electronic switch modules are shown in Fig. 2(b), where each of them consists of a bidirectional power electronic switch and some extra load. In each bidirectional power electronic switches, there are IGBTs or IGCTs, snubbers (*RC* circuitry), and overvoltage protectors/energy absorbers (metal oxide varistor—MOV). Some extra load can be added to adjust the MCFCL performance, while herein for simplification no extra load is added.

In Fig. 2(a), for generalization purpose m (an arbitrary number) power electronic switch modules are placed on the secondary side so that diverse load profiles can be achieved via various switching sequence during the current-limiting operation. However, in this article only one power electronic switch module is placed on the secondary side for simplification, having only three loading conditions (short-circuit, open-circuit, and transition between short-circuit and open-circuit). This does not weaken the reasonability and generalization of this article because the current-limiting principle and research method are the same regardless of the power electronic switch module number. Multiple power electronic switch modules can be considered to meet some specific current-limiting requirements based on this article.

Some topology similarity exists between the SI-FCL (or SI-SFCL) and MCFCL, which both contain coupled windings, while their current limiting principles are different. In SI-FCL for dc application, there are two windings, the dc reactor winding (connecting to power line) and the dc-biased winding. A current source is applied to drive the current in the dc biased winding to shift the core *B-H* characteristics. Under the normal operation the core is saturated, and hence the SI-FCL shows low inductance. Once the short-circuit fault occurs, high current goes through the dc reactor winding. As a result, the core permeability is changed, and the core moves to unsaturation region. The SI-FCL inductance increases, and the fault current is limited. Consequently, the inductance change is due to the iron core permeability change. The MCFCL inductance is changed by the secondary winding load control, which is like transformer. No power source is connected to the secondary winding. Under either normal or current limiting operation, the core saturation must be avoided because saturation disables the MCFCL inductance change, and hence leads to the current limiting failure. Compared with a Reactor FCL, a MCFCL introduces a coupled secondary winding and a power electronic switch module, which achieves the active impedance change. Moreover, in the existing VSC HVDC projects, Reactor FCLs are deployed [1], [12]—[14], which supports the reasonability to put the reactor FCL as a benchmark for the MCFCL research in this article.

From the normal operation to fault initiation and then fault clearance, the transmission line current under the MCFCL and DCCB solution (MCFCL & DCCB) is illustrated in Fig. 3. The reactor FCL and DCCB solution (Reactor FCL & DCCB), the conventional solution, is regarded as the benchmark. The period can be divided into normal operation t_{norm} and FCL operation t_{FCL}. In t_{FCL}, the MCFCL & DCCB have approximately four linear short-circuit current segments under the respective operation states. The four segments are named in time sequence as precurrent-limiting segment (S1), mode transition segment

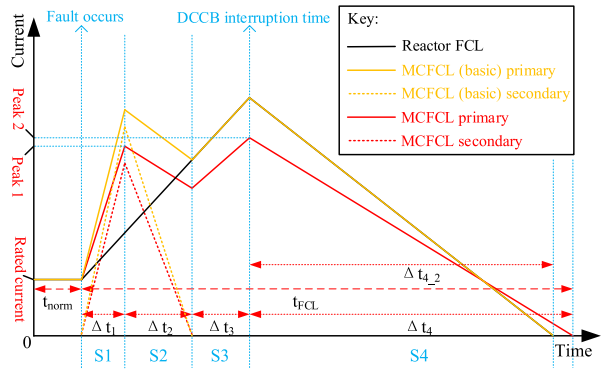

Fig. 3. Short-circuit current of MCFCL and DCCB benchmarking Reactor FCL and DCCB.

(S2), current-limiting segment (S3), and energy dissipation segment (S4). Their durations are defined as Δt_1, Δt_2, Δt_3, and Δt_4 correspondingly. For MCFCLs, the Peak 2 magnitude is determined by the primary inductance, out of which the reason is discussed in Part G. Fig. 3 shows the current of MCFCL (basic) whose primary winding self-inductance is the same with the benchmark Reactor FCL inductance. During S3 and S4, the current in MCFCL (basic) primary side is the same with the benchmark Reactor FCL. Increasing MCFCL primary winding self-inductance is a cost but necessary to reduce Peak 2. However, not like Reactor FCL this does not introduce much inductance under the normal operation. This nature is used to achieve the target MCFCL (the red curves in Fig. 3). In the following content, the "MCFCL" refers to the target MCFCL.

During S1, the MCFCL has lower impedance than the reactor FCL, because the mutual inductor secondary winding is short-circuited before the current-limiting mode is triggered. Short-circuit current rises much faster in the MCFCL, meanwhile exciting high voltage in the secondary winding. After detecting the fault and triggering the current-limiting mode, the secondary side is switched from short-circuit to open-circuit. While this cannot be switched without the mode transition segment (S2). During S2, the MOV clamps the secondary winding voltage, decreasing the secondary side current, dissipating energy, exciting negative voltage on the primary side, and hence suppressing the current rise rate in the transmission line. The current change rate during S2 depends on the MCFCL parameters. S3 starts once the secondary winding current decays to zero, open-circuited in the secondary winding. During S3, the current rise rate is slower than that of the Reactor FCL as the MCFCL primary winding inductance is designed to be higher than the Reactor FCL inductance. As a result, the DCCB interruption current under MCFCL & DCCB is lower than that under Reactor FCL & DCCB. After the DCCB interruption, the residual energy is dissipated via the DCCB MOV bank. S4 lasts for Δt_4 which is longer than the energy dissipation duration under Reactor FCL & DCCB because of the higher inductance in MCFCL (assume the same DCCB MOV bank). After S4, the MCFCL secondary winding is short-circuited again, preparing for the reclosing and the next dc fault.

Fig. 3 illustrates the MCFCL advantages over Reactor FCLs: (a) higher impedance under current-limiting mode, (b) lower

impedance under normal operation. Fig. 3(a) results in lower DCCB interruption current, and Fig. 3(b) realizes more precise dc-link voltage control and higher system dynamic characteristics.

In an air-core mutual inductor, the relation among primary self-inductance, secondary self-inductance, and mutual inductance can be simply formulated in (1). The assumption is made herein that the radial and axial lengths of the primary and secondary windings are the same hence their self-inductances are approximated to be proportional to the winding turn number. The mutual inductance is determined by the primary and secondary self-inductances and coupling factor

$$\begin{cases} n = \frac{L_{11}}{L_{22}} \\ k = \frac{M}{\sqrt{L_{11}L_{22}}} \end{cases} \tag{1}$$

where L_{11} and L_{22} are the primary and secondary self-inductances, respectively, M is the mutual inductance, n is the turns ratio between the primary and secondary windings, and k is the coupling factor.

B. Performances of Reactor FCL and MCFCL

The reason to choose the Reactor FCL as the benchmark device is discussed in the previous part. Herein it is necessary to emphasize its advantages and disadvantages, after which the proposed MCFCL is compared with Reactor FCLs and the other FCLs.

According to Table I, Reactor FCLs are low-loss, small, light, cheap, and simple. Due to its simple structure, its failure rate can be very low under proper design and it is not that meaningful to discuss its fail-safe characteristic, while its inductance cannot be changed and is high under the normal operation. The inductance to suppress fault current, on the other hand, decreases the dc-grid system dynamic characteristics or dc-link voltage control precision under normal operation. This nature constrains both its current-limiting effect and the normal operation performance.

MCFCLs achieve the active impedance control and compensate for the key disadvantages of Reactor FCLs, while the cost is the addition of a secondary winding with a power electronic switch module. Moreover, the better current-limiting effect requires more MCFCL primary winding turns. While bigger conductors can compensate for more loss introduced by more winding turns. Although the size, weight, cost, and complexity all increase in MCFCLs comparing with reactor FCLs, the benefits are critical and hence its advantages and disadvantages are more balanced as shown in Table I.

It can respond to the short-circuit fault immediately because even under normal operation or S1, some inductance remains on MCFCL. The recovery time is the same with SSFCLs. Hence, in Table I MCFCL tops different FCLs in terms of the response and recovery time. Its fail-safe characteristic depends on the secondary side load after failure. It is fail-safe if the secondary is open-circuited after failure, which can be achieved via proper power electronic device selection and protection scheme.

Although the exact size and weight are unavailable, these can be roughly estimated based on those of the Reactor FCLs and SSFCLs of the similar ratings. From industry practice, the

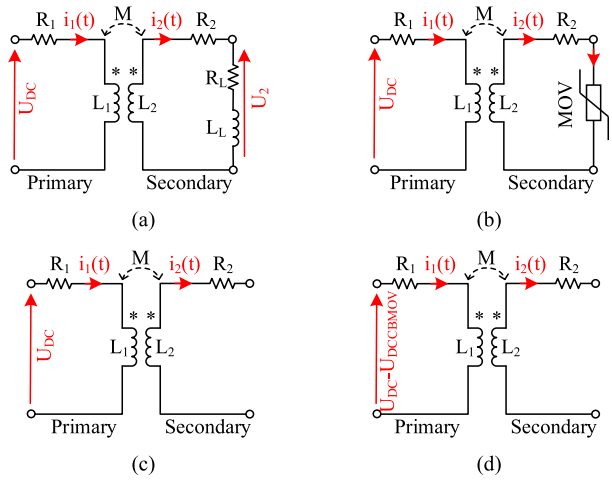

Fig. 4. MCFCL equivalent circuit models under four sequential segments. (a) S1. (b) S2. (c) S3. (d) S4.

size and weight of an MCFCL air-core mutual inductor are about twice those of an air-core Reactor FCL. Under the normal operation, the conduction loss on the secondary side power electronic devices can be negligible. Hence, the MCFCL power electronic switch module cooling system can be much smaller. It is assumed that for MCFCL power electronic switch module, 1/3 volume, and weight are reduced compared with the SSFCL under the same VA rating. Consequently, the size and weight of MCFCL are in the same level with SSFCL, ranking medium among different FCLs in Table I.

The cost is medium mainly due to the power electronic switch module. Although an MCFCL uses much more components than a Reactor FCL, either the power electronic switch module or the mutual inductor involves the technologies of this generation and is widely used in industry. Hence, its complexity and reliability are medium.

C. Modeling Conditions

The Reactor FCL & DCCB and MCFCL & DCCB current-limiting operations are qualitatively demonstrated in Section II-A. The 4-segment model is proposed here to characterize and quantify the MCFCL current-limiting operation under each of the four sequential segments. The MCFCL equivalent circuit models under S1, S2, S3, and S4 are shown in Fig. 4.

The modeling conditions are assumed as the following to simplify and generalize this four-segment model analytical study.

1) FCLs are closely connected to VSCs and no short-circuit fault occurs between VSCs and their corresponding FCLs, short-circuit current going through FCLs.
2) The worst case is defined that the short-circuit fault occurs close to a VSC without introducing any transmission line impedance into the short-circuit loop.
3) The VSC dc-link capacitance is high enough to keep the dc-link voltage unchanged during the FCL current-limiting operation.
4) The MCFCL mutual inductor is air-cored. There is no iron loss, magnetic saturation, or parameters change.

5) The parasitic capacitance and resistance in MCFCL mutual inductor are small and negligible.
6) During S1, the ON-state voltage drop is neglected in the power electronic switch module, the secondary side short-circuited.
7) The power electronic device switching transient voltage and current characteristics are not considered in detail due to its negligible effects to the current-limiting performance.
8) The current commutating among power electronic devices, *RC* circuit, and MOV is not considered in detail due to its negligible effects to the current-limiting performance.
9) During S2, the MOV clamps the secondary winding to a constant voltage till the current decays to zero.
10) During S3, the secondary winding is open-circuited, neglecting the leakage current.
11) During S4, the DCCB MOV keeps the constant voltage.

D. Reactor FCL Modeling

As the Reactor FCL is the benchmark device, it is modeled first. Before the DCCB interruption, it is modeled as follows:

$$U_{dc} = R_{FCL}\, i\,(t) + L_{FCL}\frac{di\,(t)}{dt} \tag{2}$$

where U_{dc} is the dc-link voltage, R_{FCL} is the Reactor FCL resistance, L_{FCL} is the Reactor FCL inductance, and $i(t)$ is the transmission line current. After the DCCB interruption, its modeling is the same with the MCFCL modeling during S4, which is discussed in Section II-H.

E. MCFCL Modeling During S1

The MCFCL during S1 can be modeled in (3) corresponding Fig. 4(a). S1 lasts for Δt_1 as shown in Fig. 3

$$\begin{cases} U_{dc} = L_{11}\,\frac{di_1(t)}{dt} - M\frac{di_2(t)}{dt} \\ U_2 = L_{22}\,\frac{di_2(t)}{dt} - M\frac{di_1(t)}{dt} \\ i_1\ (0) = I_{\rm rated} \\ i_2\ (0) = 0 \end{cases} \tag{3}$$

where $i_1(t)$ and $i_2(t)$ are the primary and secondary winding currents, respectively, and $I_{\rm rated}$ is the rated current. R_1 and R_2 are the parasitic resistances and neglected according to the modeling conditions, respectively. During S1 the secondary winding is short-circuited, and hence the load resistance R_L and inductance L_L are zero, $U_2 = 0$. Equation (3) can be rearranged as follows:

$$\begin{cases} U_{dc} = L_{11}\,\frac{\Delta i_1(t)}{\Delta t} - M\frac{\Delta i_2(t)}{\Delta t} \\ 0 = L_{22}\,\frac{\Delta i_2(t)}{\Delta t} - M\frac{\Delta i_1(t)}{\Delta t} \\ i_1\ (0) = I_{\rm rated} \\ i_2\ (0) = 0. \end{cases} \tag{4}$$

According to (4), the primary and secondary current rise rates during S1 can be given as

$$\begin{cases} \frac{\Delta i_1}{\Delta t} = \frac{L_{22}U_{dc}}{L_{11}L_{22}-M^2} \\ \frac{\Delta i_2}{\Delta t} = \frac{MU_{dc}}{L_{11}L_{22}-M^2} \end{cases} \tag{5}$$

which can be rearranged in a simpler form

$$\begin{cases} U_{dc} = L_{1eq}\,\frac{\Delta i_1}{\Delta t} \\ U_{dc} = L_{2eq}\,\frac{\Delta i_2}{\Delta t} \end{cases} \tag{6}$$

where

$$\begin{cases} L_{1eq} = \frac{L_{11}L_{22}-M^2}{L_2} = L_{11}\,\left(1-k^2\right) \\ L_{2eq} = \frac{L_{11}L_{22}-M^2}{M} = \frac{1-k^2}{k}\,\sqrt{L_{11}L_{22}}. \end{cases} \tag{7}$$

L_{1eq} and L_{2eq} are primary and secondary winding equivalent inductances, respectively. Hence, L_{1eq} is less than L_{11}.The explanation should be made here that L_{1eq} and L_{2eq} only have the mathematical meaning, giving the primary and secondary current rise rates under the voltage U_{dc}.

According to (5), MCFCL primary and secondary currents at the end of S1 are as follows:

$$\begin{cases} i_1\ (\Delta t_1) = I_{\rm rated}\ + \frac{U_{dc}}{L_{1eq}}\Delta t_1 \\ i_2\ (\Delta t_1) = \frac{U_{dc}}{L_{2eq}}\,\Delta t_1. \end{cases} \tag{8}$$

In Fig. 3, the primary current reaches Peak 1 and secondary current gets to its peak at the end of S1.

F. MCFCL Modeling During S2

The modeling during S2 is similar. Equations (9) and Fig. 4(b) together represent the analytical model

$$\begin{cases} U_{dc} = L_{11}\,\frac{di_1(t)}{dt} - M\frac{di_2(t)}{dt} \\ 0\ = L_{22}\,\frac{di_2(t)}{dt} - M\frac{di_1(t)}{dt} + U_{\rm MCFCL2}\,(i_2\,(t)) \end{cases} \tag{9}$$

where $U_{\rm MCFCL2}$ is the MCFCL secondary winding MOV instantaneous voltage, and it is determined by $i_2(t)$.

MOV is a nonlinear component and its voltage versus current (*V–I*) characteristics is shown in Fig. 3(a) in [30, Fig. 3(a)]. During the transition between S1 and S2, the power electronic device is switched OFF, and current commutates from the power electronic device to the *RC* circuit and then the MOV. It lasts for only several microseconds, during which current conducts on the power electronic device, *RC* circuit, and MOV [30]. This transition is neglected according to the modeling conditions. S2 begins once all the current commutates to the MOV and finishes till the MOV current decays to zero. Zhang *et al.* [30] gave examples that during the same process less than 10% variation is seen on the MOV instantaneous voltage. Hence, to simplify the analytical model, the voltage across the MOV is assumed to be constant, equal to the MOV voltage – $U_{\rm MCFCLMOV}$. As a result, this simplification decouples $U_{\rm MCFCL2}$ and i_2, supporting the following modeling and design work. Additionally, for design purpose the S2 modeling accuracy is not as important as those in S1 and S3, which relate to the MCFCL impedance under normal operation and the DCCD interruption current, respectively.

The primary and secondary current change rates can be given as follows:

$$\begin{cases} \frac{\Delta i_1}{\Delta t} = \frac{U_{dc} - \frac{M}{L_{22}} U_{\mathrm{MCFCLMOV}}}{L_{11} - \frac{M^2}{L_{22}}} \\ \frac{\Delta i_2}{\Delta t} = \frac{U_{dc} - \frac{L_{11}}{M} U_{\mathrm{MCFCLMOV}}}{\frac{L_{11} L_{22}}{M} - M} \end{cases} \tag{10}$$

which can be rewritten as

$$\begin{cases} U_{1eq} = L_{1eq} \ \frac{\Delta i_1}{\Delta t} \\ U_{2eq} = L_{2eq} \ \frac{\Delta i_2}{\Delta t} \end{cases} \tag{11}$$

where

$$\begin{cases} U_{1eq} = U_{dc} \ - \frac{M}{L_{22}} U_{\mathrm{MCFCLMOV}} \\ U_{2eq} = U_{dc} \ - \frac{L_{11}}{M} U_{\mathrm{MCFCLMOV}} \end{cases} \tag{12}$$

U_{1eq} and U_{2eq} are, respectively, the primary and secondary winding equivalent voltages during S2. They only have mathematical meanings, numerically giving the current change rates under the respective equivalent inductances L_{1eq} and L_{2eq}.

According to (11) and (12), $i_1(t)$ and $i_2(t)$ can have positive or negative current change rates that are determined by U_{1eq} and U_{2eq}. U_{1eq} and U_{2eq} are determined by U_{dc}, U_{MCFCLMOV}, L_{11}, L_{22}, and M. Among these parameters, U_{dc} is the system parameter and cannot be changed. While U_{MCFCLMOV}, L_{11}, L_{22}, and M can be designed coordinately to change the primary and secondary winding current change rates. Herein, U_{1eq} and U_{2eq} are designed to be negative to realize the negative current change rates on both $i_1(t)$ and $i_2(t)$. Moreover, the parameters are designed to decrease $i_2(t)$ to zero before the DCCB interruption as shown in Fig. 3. According to (11) the duration of S2, Δt_2, can be calculated

$$\Delta \, t_2 = \ - L_{2eq} \frac{i_2 \left(\Delta t_1 \right)}{U_{2eq}}. \tag{13}$$

The primary and secondary currents at the end of S1 are known and the currents at the end of S2 can be calculated

$$\begin{cases} i_1 \ (\Delta t_1 + \Delta t_2) = I_{\mathrm{rated}} \ + \frac{U_{dc}}{L_{1eq}} \Delta t_1 + \frac{U_{1eq}}{L_{1eq}} \Delta t_2 \\ i_2 \ (\Delta t_1 + \Delta t_2) = \ 0. \end{cases} \tag{14}$$

Substitute (8) into (13) to eliminate $i_2(\Delta t_1)$ and then substitute Δt_2 into (14) to give

$$\begin{cases} i_1 \ (\Delta t_1 + \Delta t_2) = I_{\mathrm{rated}} \ + \frac{U_{dc}}{L_{1eq}} \Delta t_1 + \frac{U_{1eq}}{L_{1eq}} \left(\frac{U_{dc}}{-U_{2eq}} \Delta t_1 \right) \\ i_2 \ (\Delta t_1 + \Delta t_2) = \ 0 \end{cases} \tag{15}$$

that $i_1(\Delta t_1 + \Delta t_2)$ is decoupled with Δt_2.

G. MCFCL Modeling During S3

During S3, the secondary winding is open-circuited, and the MCFCL shows the primary winding self-inductance, as shown in Fig. 4(c). The MCFCL during S3 can be modeled

$$U_{dc} = L_{11} \ \frac{di_1 \left(t \right)}{dt} \tag{16}$$

which can be linearized

$$\frac{\Delta i_1}{\Delta t} = \frac{U_{dc}}{L_{11}}. \tag{17}$$

Hence, the primary and secondary currents at the end of S3, the DCCB interruption time, can be given by (18), where $t_3 = \Delta t_1 + \Delta t_2 + \Delta t_3$. At the instant the MCFCL primary winding current gets to Peak 2, as shown in Fig. 3

$$\begin{cases} i_1 \ (t_3) = i_1 \ (\Delta t_1 + \Delta t_2) + \frac{U_{dc}}{L_{11}} \left[t_3 - \Delta i_1 + \frac{U_{dc}}{-U_{2eq}} \Delta i_1 \right] \\ i_2 \ (t_3) = \ 0. \end{cases} \tag{18}$$

The MCFCL primary winding current at t_3 is the DCCB interruption current I_{DCCB}. Substitute (15) into (18) and rearrange the equation to obtain

$$\begin{cases} i_1 \ (t_3) = I_{\mathrm{rated}} \ + \left[\frac{U_{dc}}{L_{1eq}} \left(1 - \frac{U_{1eq}}{U_{2eq}} \right) - \frac{U_{dc}}{L_{11}} \left(1 + \frac{U_{dc}}{U_{2eq}} \right) \right] \\ \quad \Delta i_1 + \frac{U_{dc}}{L_{11}} t_3 \\ i_2 \ (t_3) = \ 0 \end{cases} \tag{19}$$

where the DCCB interruption current is the sum of three components, the rated current I_{rated}, the component with Δi_1, and the component with t_3. Substitute U_{1eq}, U_{2eq}, and L_{1eq} into the component with Δi_1 to obtain

$$\frac{U_{dc}}{L_{1eq}} \left(1 - \frac{U_{1eq}}{U_{2eq}} \right) - \frac{U_{dc}}{L_{11}} \ \left(1 + \frac{U_{dc}}{U_{2eq}} \right) = \ 0 \tag{20}$$

which indicates the DCCB interruption current is the sum of the rated current I_{rated} and the component with t_3

$$\begin{cases} i_1 \ (t_3) = I_{\mathrm{rated}} \ + \frac{U_{dc}}{L_{11}} t_3 \\ i_2 \ (t_3) = \ 0 \end{cases} \tag{21}$$

where U_{dc}, I_{rated}, and t_3 are system parameters and DCCD interruption time. Consequently, for MCFCLs it is L_{11} that determines the DCCB interruption current.

H. MCFCL Modeling During S4

The short-circuit current is interrupted by DCCB, ending S3 and starting S4 as shown in Fig. 3. The DCCB MOV starts to dissipate the residual energy in MCFCL. During S4, the MCFCL shows the primary winding self-inductance, and the voltage seen by the MCFCL is changed, as shown in Fig. 4(d). The analytical model is as follows:

$$\begin{cases} U_{dc} = L_{11} \ \frac{di_1(t)}{dt} + U_{\mathbf{DCCBMOV}} \\ i_2 \ (t) = \ 0 \end{cases} \tag{22}$$

where U_{DCCBMOV} is the DCCB MOV voltage.

L_{11} is higher (to increase the suppressing effect) than L_{FCL}, resulting in slower current decrease rate for the MCFCL as shown in Fig. 3. According to (21) and (22), the duration of S4, Δt_4, can be calculated as follows:

$$\Delta \, t_4 = \frac{L_{11} I_{\mathbf{rated}} + U_{dc} t_3}{U_{dc} - U_{\mathbf{DCCBMOV}}} \ . \tag{23}$$

While for the Reactor FCL, the duration from the DCCB interruption to the current zero crossing point Δt_{4_2}, as shown in Fig. 3, can be calculated via

$$\Delta \, t_{4\_2} = \frac{L_{FCL} I_{\mathbf{rated}} + U_{dc} t_3}{U_{dc} - U_{\mathbf{DCCBMOV}}} \ . \tag{24}$$

TABLE II
REACTOR FCL & DCCB AND MCFCL & DCCB SPECIFICATIONS UNDER A MEDIUM VOLTAGE CASE

System parameters	DC-link voltage U_{dc} (kV)	10
	Rated current I_{rated} (kA)	1
	DCCB interruption time t_{DCCB} (ms)	3
Reactor FCL & DCCB	Inductance L_{FCL} (mH)	5
	Resistance R_{FCL} (mΩ)	10
	DCCB interruption current I_{DCCB} (kA)	7.4
	DCCB MOV $U_{DCCBMOV}$ (kV)	14
MCFCL & DCCB	Primary self-inductance L_{11} (mH)	8
	Primary resistance R_1 (mΩ)	10
	Secondary self-inductance L_{22} (mH)	4
	Secondary resistance R_2 (mΩ)	10
	Coupling factor k	0.9
	MCFCL trigger time Δt_1 (ms)	0.5
	DCCB interruption current I_{DCCB} (kA)	5
	DCCB MOV $U_{DCCBMOV}$ (kV)	14
	MCFCL MOV $U_{MCFCLMOV}$ (kV)	10

The current suppression time is defined as the time from fault initiation to current zero crossing point. According to the above discussion $\Delta t_1 + \Delta t_2 + \Delta t_3 + \Delta t_{4\_2} < \Delta t_1 + \Delta t_2 + \Delta t_3 + \Delta t_4$, the current suppression time of an MCFCL is longer than that of a Reactor FCL. However, this does not add much, e.g., less than 1ms in the case study in Section III. 1 ms is not much compared with the whole current suppression process.

III. MCFCL DESIGN CASE STUDY

One MCFCL is designed under a medium voltage (10 kV) case, benchmarking a Reactor FCL. The system and Reactor FCL specifications are shown in Table II. The improvement goals via the MCFCL implementation are defined: 1) decrease the DCCB interruption current by no less than 30%; and 2) decrease the FCL inductance under normal operation by no less than 50%, both benchmarking the Reactor FCL.

From the MCFCL 4-segment model, its design covers five parameters L_{11}, k, Δt_1, L_{22}, and U_{MCFCLMOV}. L_{11} determines the DCCB interruption current; the MCFCL equivalent impedance under normal operation partially depends on k; the Peak 1 magnitude is linked with Δt_1; the secondary winding peak current relates to L_{22}; and during S2, the primary and secondary winding current change rates relate to U_{MCFCLMOV}. Fig. 5 gives a view of the MCFCL design procedure.

It is assumed that the transmission line current keeps the rated current before fault, and the DCCB interruption time is 3 ms after fault. The Reactor FCL impedance is 5 mH. Hence, the DCCB interruption current is 7 kA. According to industrial practice, 5% derating should be considered in the DCCB interruption capability, resulting in its rating –7.4 kA. Based on (21), design L_{11} to be 1.6 times the Reactor FCL inductance, resulting in $L_{11} = 8$ mH. The DCCB interruption current becomes 4.75 kA, and the 5% derating leads to the DCCB rating – 5 kA. This is 67.6% of that with the Reactor FCL (7.4 kA). The first improvement goal is fulfilled. The MCFCL performance sensitivity to L_{11} is analyzed via the four-segment

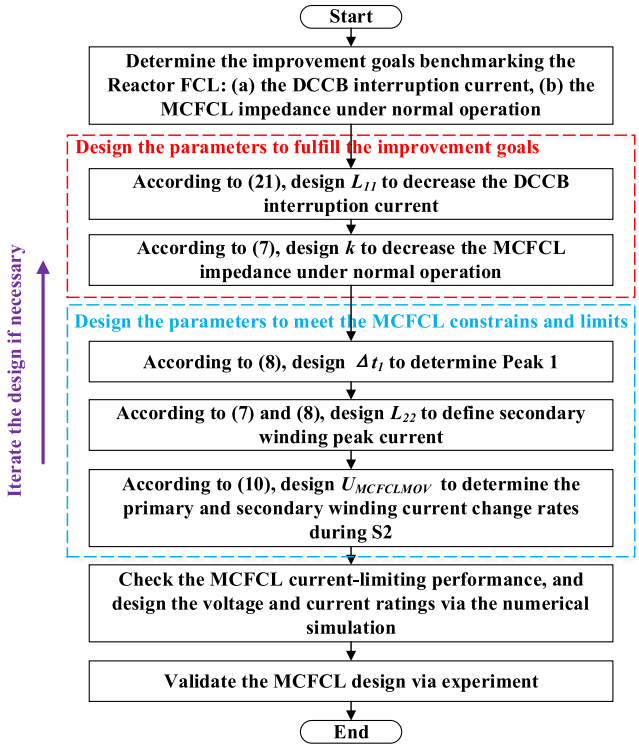

Fig. 5 MCFCL design procedure.

model, as shown in Fig. 6(a). Higher L_{11} leads to lower primary and secondary winding currents, and higher impedance under normal operation. The other parameters supporting the four-segment model analysis are shown in Table II.

After the design of L_{11}, based on (7) design k to be 0.83 to achieve that the MCFCL inductance under normal operation is 50% the Reactor FCL inductance. For design margin consideration, herein the coupling factor is designed to be 0.90 corresponding 69.6% impedance decrease. The second improvement goal is achieved. Fig. 6(b) shows the MCFCL performance sensitivity to k that higher k results in lower impedance under normal operation.

Peak 1 is not supposed to be higher than Peak 2 to avoid the possible VSC blocking before the DCCB interruption, which is an MCFCL design constraint. After the design of L_{11} and k, according to (8) the MCFCL trigger time Δt_1 is designed to be 0.5 ms. The Peak 1 sensitivity to Δt_1 is shown in Fig. 6(c). In [9], an SSFCL response time, from fault detection to the current limiting behavior initiation, is 0.1 ms. Hence, 0.5 ms is a reasonable time for the fault detection, decision, and action.

So far, L_{11}, k, and $\Delta t_1$are designed. Based on (7) and (8), the next parameter to be designed is L_{22}, which relates to the secondary winding peak current as shown in Fig. 6(d). Based on (10), the final parameter to be designed is U_{MCFCLMOV} relating to the primary and secondary winding current change rates during S2 as shown in Fig. 6(e). Consequently, the MCFCL parameters are shown in Table II.

Although *RC* snubber parameter design and power electronic semiconductor device selection are not the focus of this article, they determine the MCFCL transient performance on the power

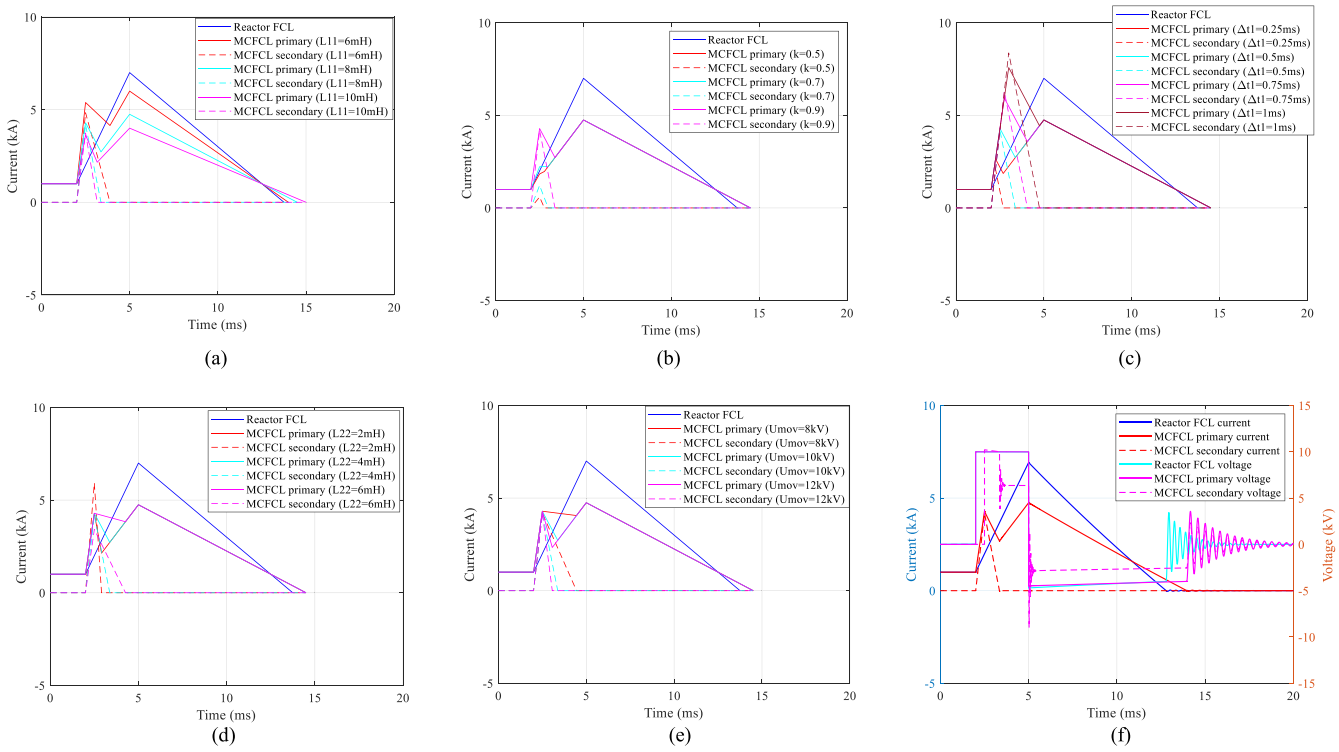

Fig. 6 Current-limiting performance sensitivities to parameters and numerical model simulation result. (a) Primary winding inductance. (b) Coupling factor. (c) Trigger Time. (d) Secondary winding inductance. (e) MOV voltage. (f) Numerical model simulation.

electronic device switching instant and should be properly considered. In the hybrid DCCB design, the RC snubber circuitry design method can be found in [30], and the power electronic semiconductor device selection principle in [31], which can both be used in MCFCL power electronic switch module design. The MCFCL primary and secondary winding transient voltage waveforms are shown in Fig. 6(f) via the numerical model built in MATLAB Simulink using the similar *RC* parameters in the corresponding voltage and current levels in [30]. The voltage and current ratings should be considered during the design.

IV. Experimental Validation

In the previous section, one MCFCL is designed, and its current-limiting performance, transient voltage, and current are checked via the numerical model. Herein a scaled-down experimental facility is built to validate the numerical model (its correctness and accuracy), after which the MCFCL study is validated.

The experimental facility overview is shown in Fig. 7(a). Table III shows the scaled-down experimental facility specifications, and Fig. 7(b) illustrates its topology. The experimental facility consists of one dc power source, one 200-Ω protective resistor to limit charging current, a 15-mF dc-link capacitor bank, a DCCB, and the device under test (DUT)—MCFCL. One IGBT power electronic switch module (IGBT: Infineon FZ1600R17KE3) as shown in Fig. 2(b) is used as the DCCB, and the other one is used to control the MCFCL secondary side impedance. The dc-link capacitor is slowly charged up to 550 V via the dc power source and 200-Ω protective resistor. To reproduce the short-circuit current, the DCCB is switched ON to discharge the dc-link capacitor, from zero the current increases drastically. The MCFCL is triggered to limit the current rise rate, and the short-circuit current is interrupted by the DCCB 3 ms after fault.

Table III
Scaled-Down Experimental Facility Specifications

System parameters	DC-link voltage U_{dc} (V)	550
	DCCB interruption time t_{DCCB} (ms)	3
Reactor FCL & DCCB	Inductance L_{FCL} (mH)	2.33
	Resistance R_{FCL} (mΩ)	264
	DCCB MOV $U_{DCCBMOV}$ (V)	680
MCFCL & DCCB	Primary self-inductance L_{11} (mH)	3.31
	Primary resistance R_1 (mΩ)	295
	Secondary self-inductance L_{22} (mH)	2.33
	Secondary resistance R_2 (mΩ)	264
	Coupling factor k	0.85
	MCFCL trigger time Δt_1 (ms)	0.75
	MCFCL MOV $U_{MCFCLMOV}$ (V)	470
	DCCB MOV $U_{DCCBMOV}$ (V)	680

The reproduced short-circuit current in the experimental facility is supposed to be as high as possible to emulate the FCL short-circuit current suppression physics in VSC dc grids. The benchmark Reactor FCL is chosen to be 2.33 mH. The improvement goals are defined: 1) decrease the DCCB interruption current by no less than 30%; and 2) decrease the FCL inductance

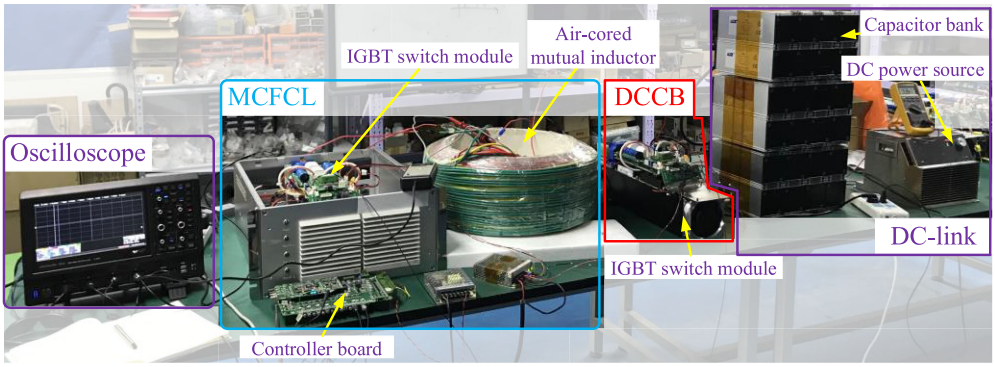

(a)

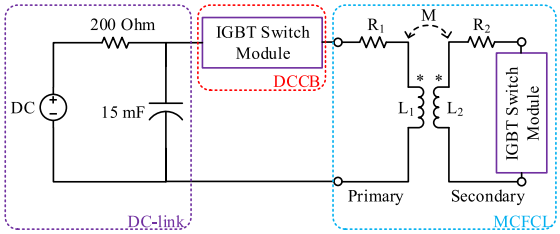

(b)

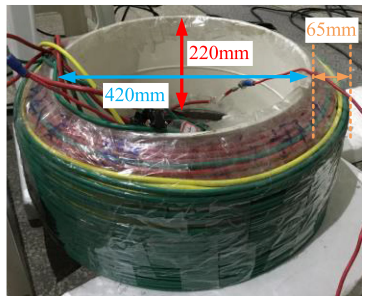

(c)

Fig. 7 Experimental facility. (a) Overview. (b) Topology. (c) Mutual inductor.

under normal operation by no less than 50%, both benchmarking the Reactor FCL. According to the MCFCL design method, the parameters are designed, as shown in Table III. The note should be made that to guarantee the MCFCL improvement goals, some gaps are considered in the parameter design margins.

Based on the design parameters, as shown in Fig. 7(c), the MCFCL mutual inductor is wound by the insulated cable whose diameter is 6.42 mm. The cable has the stranded round conductor made of 49 copper wires, of which each has the diameter 0.54 mm. Ten single layer coils (total thickness 65 mm) are wound concentrically in the same direction on a plastic tube (diameter 420 mm and height 220 mm), and from inner to outer side the coils are named as coil 1, coil 2, … and coil 10. Coils 1, 3, and 5 are connected in series in the same direction to make the primary winding (84 turns), and coil 6, 8, and 10 are connected in series in the same direction to make the secondary winding (61 turns). In MCFCL, the primary and secondary windings are mutually coupled in the direction, as shown in Fig. 2(a). Due to the measurement from LCR meter, the primary and secondary winding dc resistances are 295 and 264 mΩ; the primary and secondary winding self-inductances are 3.31 and 2.33 mH; and if the other side winding is short-circuited, the primary and secondary side inductances are 950 and 653 μH, respectively. Connect the primary and secondary windings in series under cumulatively coupled and differentially coupled forms and measure the inductances. The measurements are 10.40 mH and 931μH, respectively. Hence, the mutual inductance is 2.37 mH and the coupling factor is 0.85.

The numerical model is built according to the scaled-down experimental facility specifications, and the simulation results are shown in Fig. 8. The designed MCFCL shows better current-limiting effect than the Reactor FCL, as shown in Fig. 8(a)–(c). In Fig. 8(c) the MCFCL current-limiting effect under different trigger time (0.25, 0.5, 0.75, and 1 ms) are also compared, benchmarking the Reactor FCL. The Peak 1 magnitude increases with the rise of MCFCL trigger time, while regardless of the MCFCL trigger time, the DCCB interruption currents do not change. Peak 1 magnitude rises if MCFCL trigger time increases; and it overtakes Peak 2 at $\Delta t_1 =$ 1ms, which should be avoided. Hence, $\Delta t_1 =$ 0.75ms is designed compromising the Peak 1 constrain and enough fault response time (fault detection, protection decision, and action delay, etc.). As a result, benchmarking the DCCB interruption current under the Reactor FCL (570 A), a 30% decrease is achieved via the MCFCL implementation, resulting in 400 A. Moreover, during S1 the current rise rate with the MCFCL is twice that with the Reactor FCL, indicating its 50% impedance decrease under normal operation. The improvement goals are achieved.

The numerical model is validated via this experiment, and the experimental results are shown in Fig. 9. Although some slight differences occur, the numerical model simulation and experimental results match.

For both the Reactor FCL and MCFCL in the experiment, parasitic resistances, R_1 and R_2, are inevitably introduced via inductor winding cable. Moreover, the dc-link voltage drops other than keeps constant during short-circuit current discharging. This results in some difference, i.e., nonlinear short-circuit current rise, compared with that in the four-segment model, as shown in Fig. 6. The reason is that in the four-segment model, the parasitic resistance is neglected, and the dc-link voltage is

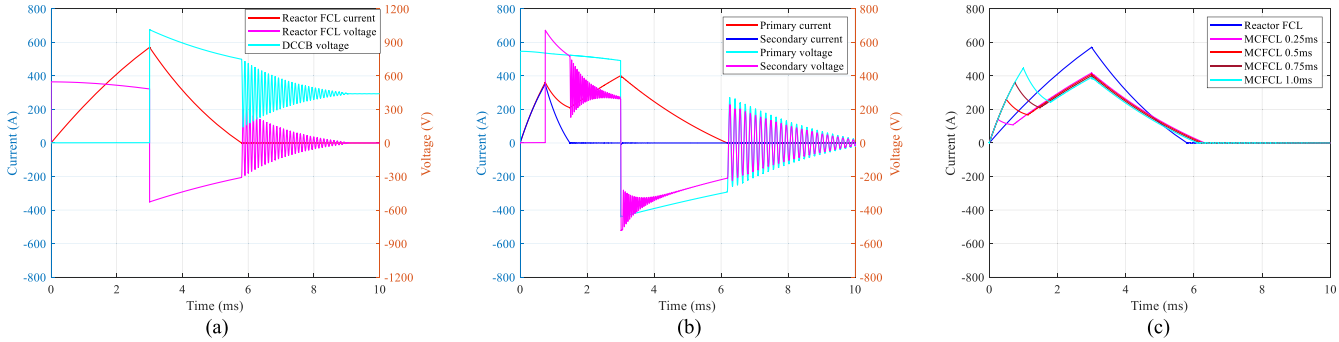

Fig. 8 Simulation results. (a) Reactor FCL. (b) MCFCL. (c) Current-limiting performance comparison.

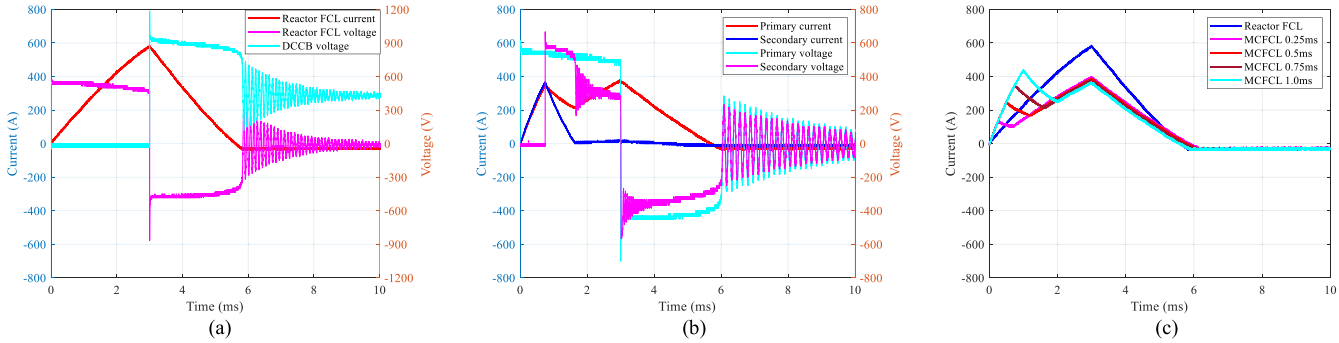

Fig. 9 Experimental results. (a) Reactor FCL. (b) MCFCL. (c) Current-limiting performance comparison.

assumed to be constant during the current-limiting operation. However, this mismatch will not undermine the experimental validation because the experimental facility and the numerical model have the same parameters, and their results match. The note should be made according to industrial experience, the smoothing reactor parasitic resistance in LCC-HVdc transmission system can be around 10 mΩ. Similarly, this parasitic resistance level can be reasonably achieved in the MCFCL and Reactor FCL manufacturing. For the 10 mΩ level, the parasitic resistance can be neglected in MCFCL and Reactor FCL current-limiting effect analyses. For example, in Fig. 6 the 10-mΩ parasitic resistance is neglected in the four-segment model while considered in the numerical model. However, their current-limiting effect difference is too tiny to be distinguished.

Additionally, although the current and voltage waveform envelopes are almost the same between the simulation results in Fig. 8 and experimental results in Fig. 9, some slight differences occur on some local parts of the voltage and current waveforms. One possible reason is that the MOV is modeled via a simplified linear method, approximating its real-world performance. Another possible reason is that the MOV parameters are chosen under the worst case within the tolerance margin in the MOV data sheet and may differ from those of the exactly used MOVs in this experimental facility. However, the slight differences are tolerable and do not weaken the correctness and accuracy of the numerical model in the MCFCL simulation and design.

V. Conclusion

A novel MCFCL for VSC dc grids is proposed in this article. Not like the other FCLs, the concept behind MCFCL is not to pursue the excellence in one or two advantages, but to properly balance the advantages and disadvantages. Its loss, impedance under normal operation, impedance controllability, response time, recovery time, and inherent fail-safe characteristics top the different FCLs, which indicates a good electrical performance. Moreover, its size, weight, cost, complexity, and reliability rank medium among different FCLs. Consequently, this results in a good overall performance.

The novel four-segment model is proposed to model MCFCLs during current-limiting operation, and the design procedure is also proposed for MCFCLs. An MCFCL design case is carried out under a medium voltage (10 kV) application, and the MCFCL parameters sensitivities are analyzed based on the four-segment model. The voltage and current during MCFCL current-limiting operation are checked via the numerical model. The designed MCFCL achieves the improvement goals: 1) decrease the DCCB interruption current by no less than 30%; and 2) decrease the FCL inductance under normal operation by no less than 50%, both benchmarking the Reactor FCL.

A scaled-down experimental facility is built to emulate the short-circuit fault in VSC dc grids and successfully validates the numerical model. Consequently, this article, containing MCFCL

topology, modeling, design case study, and experimental validation, shows good current-suppressing effect and advantages of the novel MCFCL.

REFERENCES

[1] D. Jovcic, G. Tang, and H. Pang, "Adopting circuit breakers for high-voltage dc networks: Appropriating the vast advantages of dc transmission grids," *IEEE Power Energy Mag.*, vol. 17, no. 3, pp. 82–93, May/Jun. 2019.

[2] X. Pei, A. C. Smith, and M. Barnes, "Superconducting fault current limiters for HVDC systems," *Energy Procedia*, vol. 80, pp. 47–55, 2015.

[3] F. Jiang *et al.*, "Design consideration of a dual-functional bridge-type fault current limiter," *IEEE J. Emerg. Sel. Topics Power Electron.*, to be published.

[4] S. Eckroad, "Survey of fault current limiter (FCL) technologies," 2005. [Online]. Available: https://www.epri.com/research/products/000000000001010760. Accessed: Jul. 16, 2020.

[5] H. Lee, M. Asif, K. Park, and B. Lee, "Feasible application study of several types of superconducting fault current limiters in HVDC grids," *IEEE Trans. Appl. Supercond.*, vol. 28, no. 4, Jun. 2018, Art. no. 5601205.

[6] Q. Qiu *et al.*, "Design and test of 40-kV/2-kA DC superconducting fault current limiter," *IEEE Trans. Appl. Supercond.*, vol. 30, no. 6, Sep. 2020, Art. no. 5602305.

[7] S. Eckroad, "Superconducting fault current limiters," 2009. [Online]. Available: https://www.epri.com/research/products/000000000001017-793. Accessed: Jul. 14, 2020.

[8] Beijing Power Equipment Group, "Dry type air core reactors," 2003. [Online]. Available: http://www.bpeg.cn/dkq.pdf . Accessed: Jul. 14, 2020.

[9] R. Adapa, "Solid-state fault current limiter development," 2011. [Online]. Available: https://www.epri.com/research/products/000000000001021-916. Accessed: Jul. 15, 2020.

[10] H. Zhou, J. Yuan, F. Chen, and B. Chen, "Inductive fault current limiters in VSC-HVDC systems: A review," *IEEE Access*, vol. 8, pp. 38185–38197, 2020.

[11] J. Sun *et al.*, "Design and performance test of a 20-kV DC superconducting fault current limiter," *IEEE Trans. Appl. Supercond.*, vol. 30, no. 2, Mar. 2020, Art. no. 5600305.

[12] G. Tang, Z. He, H. Pang, X. Huang, and X. Zhang, "Basic topology and key devices of the five-terminal DC grid," *CSEE J. Power Energy Syst.*, vol. 1, no. 2, pp. 22–35, 2015.

[13] X. Han, W. Sima, M. Yang, L. Li, T. Yuan, and Y. Si, "Transient characteristics under ground and short-circuit faults in a ±500kV MMC-based HVDC system with hybrid DC circuit breakers," *IEEE Trans. Power Del.*, vol. 33, no. 3, pp. 1378–1387, Jun. 2018.

[14] X. Yu and L. Xiao, "A DC fault protection scheme for MMC-HVDC grids using new directional criterion," *IEEE Trans. Power Del.*, to be published.

[15] A. Abramovitz and K. M. Smedley, "Survey of solid-state fault current limiters," *IEEE Trans. Power Electron.*, vol. 27, no. 6, pp. 2770–2782, Jun. 2012.

[16] A. Heidary, H. Radmanesh, K. Rouzbehi, and J. Pou, "A DC-reactor-based solid-state fault current limiter for HVDC applications," *IEEE Trans. Power Del.*, vol. 34, no. 2, pp. 720–728, Apr. 2019.

[17] Z. Fu *et al.*, "A mutual-inductance-type fault current limiter in MMC-HVDC systems," *IEEE Trans. Power Del.*, vol. 35, no. 5, pp. 2403–2413, Oct. 2020, doi: 10.1109/TPWRD.2020.2967837.

[18] M. Pannu, Y. Valent, and U. Garbi, "Pre-saturated core fault current limiter," in *Proc. Australas. Univ. Power Eng. Conf.*, 2013, pp. 1–7.

[19] H. Zhou, J. Yuan, F. Chen, B. Chen, and K. Muramatsu, "Performance investigation on a novel high inductance changing ratio MMC-based direct current system saturated core FCL," *IEEE Trans. Power Del.*, vol. 35, no. 3, pp. 1502–1514, Jun. 2020.

[20] J. Yuan *et al.*, "A novel hybrid saturated core fault current limiter topology considering permanent magnet stability and performance," *IEEE Trans. Magn.*, vol. 53, no. 6, Jun. 2017, Art. no. 8400304.

[21] H. He *et al.*, "Study of liquid metal fault current limiter for medium-voltage DC power systems," *IEEE Trans. Compon., Packag. Manuf. Technol.*, vol. 8, no. 8, pp. 1391–1400, Aug. 2018.

[22] S. Eckroad, "Survey of fault current limiter (FCL) technologies—update," 2008. [Online]. Available: https://www.epri.com/research/products/1016389. Accessed: Jul. 14, 2020.

[23] J. Xu, X. Zhao, N. Han, J. Liang, and C. Zhao, "A thyristor-based DC fault current limiter with inductor inserting–bypassing capability," *IEEE J. Emerg. Sel. Topics Power Electron.*, vol. 7, no. 3, pp. 1748–1757, Sep. 2019.

[24] B. Li, J. He, Y. Li, W. Wen, and B. Li, "A novel current-commutation-based FCL for the flexible DC grid," *IEEE Trans. Power Electron.*, vol. 35, no. 1, pp. 591–606, Jan. 2020.

[25] ABB, "Fault current limiter Is-limiter," 2020. [Online]. Available: https://new.abb.com/medium-voltage/apparatus/fault-current-limiters/current-limiter. Accessed: Jul. 18, 2020.

[26] F. Jiang, C. Tu, Z. Shuai, M. Cheng, Z. Lan, and F. Xiao, "Multilevel cascaded-type dynamic voltage restorer with fault current-limiting function," *IEEE Trans. Power Del.*, vol. 31, no. 3, pp. 1261–1269, Jun. 2016.

[27] H. Nourmohamadi, M. Sabahi, P. T. Balsara, E. Babaei, S. H. Hosseini, and A. Fakhim-Babaei, "New concept for fault current limiter with voltage restoration capability," *IEEE Trans. Ind. Electron.*, vol. 67, no. 12, pp. 10001–10010, Dec. 2020.

[28] S. Chen, P. Li, R. Ball, J. Palma, and B. Lehman, "Analysis of a switched impedance transformer-type nonsuperconducting fault current limiter," *IEEE Trans. Power Electron.*, vol. 30, no. 4, pp. 1925–1936, Apr. 2015.

[29] H. Radmanesh and S. H. Fathi, "Fast AC reactor-based fault current limiters application in distribution network," *High Volt.*, vol. 3, no. 3, pp. 232–243, 2018.

[30] X. Zhang, Z. Yu, Z. Chen, Y. Huang, B. Zhao, and R. Zeng, "Modular design methodology of DC breaker based on discrete metal oxide varistors with series power electronic devices for HVDC application," *IEEE Trans. Ind. Electron.*, vol. 66, no. 10, pp. 7653–7662, Oct. 2019.

[31] Z. Chen *et al.*, "Analysis and experiments for IGBT, IEGT, and IGCT in hybrid DC circuit breaker," *IEEE Trans. Ind. Electron.*, vol. 65, no. 4, pp. 2883–2892, Apr. 2018.

Zipan Nie was born in Shandong, China in 1989. He received the B.S. degree in electrical engineering and automation from East China University of Science and Technology, Shanghai, China, in 2012, the M.S. degree in electrical energy conversion systems from the University of Manchester, Manchester, U.K., in 2013, and the Ph.D. degree in electrical and computer engineering from McMaster University, Hamilton, ON, Canada, in 2018.

From 2013 to 2014, he was an Aircraft Electrified Rudder System Design Engineer with Shanghai Academy of Spaceflight Technology, China Aerospace Science and Technology Corporation. Since 2018, he has been a Postdoctoral Research Associate with the Department of Electrical Engineering, Tsinghua University, Beijing, China. His research interests include VSC dc grids and multiphase machine drive systems.

Zhanqing Yu (Member, IEEE) was born in Inner Mongolia, China, in 1981. He received the B.Sc. and Ph.D. degrees from the Department of Electrical Engineering, Tsinghua University, Beijing, China, in 2003 and 2008, respectively.

In 2008, he became a Postdoctoral with the Department of Electrical Engineering, Tsinghua University, Beijing, China, where he became a Lecturer in 2010, an Associate Professor in December 2012. He has participated in several projects sponsored by High-Tech R&D Program (863 Program), National Basic Research Program of China (973 Program), National Natural Science Foundation of China. His research interests include dc grid, dc breaker, electromagnetic environment and electromagnetic compatibility, lightning protection.

Zhizheng Gan was born in Guangxi, China in 1998. He is currently working toward the Ph.D. degree in electrical engineering with Tsinghua University, Beijing, China.

His main research interests include the hybrid dc circuit breaker and arc characteristics.

Lu Qu (Member, IEEE) was born in 1987. He received the Ph.D. degree in electrical engineering from the University of Chinese Academy of Sciences, Hefei, China, in 2016.

He is currently a Postdoctoral Researcher with Tsinghua University, Beijing, China. His research interests include dc breaking technology, dc current limiting technology, and dc grid technology.

Yulong Huang (Member, IEEE) was born in Hubei, China, in 1964. He received the B.Eng. degree in electrical engineering from Hunan University, Changsha, China, in 1985 and the M.Sc. degree from the Department of Electrical Engineering, Tsinghua University, Beijing, China, in 1991.

He was a Visiting Scholar with the University of Manchester (formerly UMIST), Manchester, U.K., from 2000 to 2001. He is currently an Associate Professor with the Department of Electrical Engineering, Tsinghua University, working on high-voltage apparatus and new technology,

Biao Zhao (Senior Member, IEEE) was born in Hubei, China, in 1987. He received the B.S. degree from the Department of Electrical Engineering, Dalian University of Technology, Dalian, China, in 2009, and the Ph.D. degree from the Department of Electrical Engineering, Tsinghua University, Beijing, China, in 2014.

He is currently an Associate Professor with the Department of Electrical Engineering, Tsinghua University, Beijing, China. His current research interests include high power converters, high-power semiconductor devices, and flexible dc transmission and distribution systems.

Dr. Zhao is a Senior Member of the Chinese Society for Electrical Engineering and the Chinese Electro-Technical Society.